

# Creep Crack Growth Behavior of Alloys 617 and 800H in Air and Impure Helium Environments at High Temperatures



D.S. GRIERSON, G. CAO, P. BROOKS, P. PEZZI, A. GLAUDELL, D. KUETTEL, G. FISCHER, T. ALLEN, K. SRIDHARAN, and W.C. CRONE

The environmental degradation of intermediate heat exchanger (IHx) materials in impure helium has been identified as an area with major ramifications on the design of very high-temperature reactors (VHTR). It has been reported that in some helium environments, non-ductile failure is a significant failure mode for Alloy 617 with long-term elevated-temperature service. Non-ductile failure of intermediate exchangers can result in catastrophic consequences; unfortunately, the knowledge of creep crack initiation and creep crack growth (CCG) in candidate alloys is limited. Current codes and code cases for the candidate alloys do not provide specific guidelines for effects of impure helium on the high-temperature behavior. The work reported here explores creep crack growth characterization of Alloy 617 and Alloy 800H at elevated temperatures in air and in impure helium environments, providing information on the reliability of these alloys in VHTR for long-term service. Alloy 617 was found to exhibit superior CCG resistance compared to Alloy 800H. For Alloy 617 tested at 973 K (700 °C), a notable increase in the resistance to crack growth was measured in air compared to that measured in the helium environment; CCG results for Alloy 800H suggest that air and helium environments produce similar behavior. Testing of grain boundary-engineered (GBE) Alloy 617 samples revealed that, although the technique produces superior mechanical properties in many respects, the GBE samples exhibited inferior resistance to creep crack growth compared to the other Alloy 617 samples tested under similar conditions. Grain size is noted as a confounding factor in creep crack growth resistance.

DOI: 10.1007/s40553-016-0102-0

© ASM International (ASM) and The Minerals, Metals & Materials Society (TMS) 2016

## I. INTRODUCTION

IMPURE helium environments are commonly found in Next-Generation Nuclear Plants (NGNPs). NGNPs consist of generation IV very high-temperature reactors (VHTR) connected to a neighboring hydrogen production facility. Using this unique combination, NGNPs are able to produce both electricity through nuclear fission and hydrogen with high-temperature electrolysis using excess heat from the reactor.<sup>[1]</sup> The favored VHTR coolant is helium due to its good heat transfer characteristics and chemical inertness. Additionally, exposing helium to neutron radiation does not make it radioactive, unlike most other possible coolants.<sup>[2]</sup> The maximum helium coolant temperature in the

high-temperature reactor is expected to be between 1123 K and 1273 K (850 °C and 1000 °C), although early prototype designs may use a lower maximum temperature.<sup>[3]</sup> Unfortunately, the helium coolant in VHTR inevitably contains low levels of impurities during steady-state operation. The primary impurities are small amounts of H<sub>2</sub>, H<sub>2</sub>O, CH<sub>4</sub>, CO, CO<sub>2</sub>, and N<sub>2</sub>, which come from a variety of sources in the reactor circuit, such as reactions of ingressed water and oil with the core graphite, and contamination during outgassing of the reactor materials. These gaseous impurities are generally in ppm levels within the helium coolant. Previous investigations from a variety of sources indicated that a typical helium gas contains around 0.1-10 Pa H<sub>2</sub>, 0.05-45 Pa CO, 0.1-1 Pa CH<sub>4</sub>, 0.02-1 Pa CO<sub>2</sub>, 0.01-1 Pa H<sub>2</sub>O, and 0.05-22 Pa N<sub>2</sub>.<sup>[4]</sup> While the concentration of these impurities is quite low, they nevertheless can induce corrosion in the long-term, which can affect mechanical properties, particularly crack initiation at the surface and crack growth.

The primary materials under consideration for VHTR components have been Alloy 617, Haynes 230, Alloy 800H, and Hastelloy X due to their exceptional combination of high-temperature strength and oxidation resistance.<sup>[5]</sup> Regardless of alloy choice, the reactor components will ultimately experience significant long-term corrosion caused by the unwanted gaseous

---

D.S. GRIERSON, Visiting Scientist, G. CAO, Research Scientist, P. BROOKS, Senior Instrumentation Specialist, P. PEZZI and A. GLAUDELL, Undergraduate Research Assistants, T. ALLEN, Professor, K. SRIDHARAN, Distinguished Research Professor, and W.C. CRONE, Professor, are with the Department of Engineering Physics, University of Wisconsin-Madison, 1500 Engineering Dr., Madison, WI 53706. Contact e-mails: kumar.sridharan@wisc.edu, wcrone@wisc.edu D. KUETTEL and G. FISCHER, Undergraduate Research Assistants, are with the Department of Mechanical Engineering, University of Wisconsin-Madison.

Manuscript submitted May 24, 2016.

Article published online November 28, 2016

impurities, which may be exacerbated at the elevated temperatures in VHTR. Material corrosion may involve oxidation, carburization, or decarburization depending on temperature, oxygen partial pressure, carbon activity, and alloy composition. Previously, several independent high-temperature corrosion tests have been carried out to determine the extent of impure helium corrosion on the above-mentioned alloys. These tests were performed at temperatures between 1123 K and 1373 K (850 °C and 1100 °C) and revealed that all alloys exhibited a parabolic oxidation behavior characterized by chromium-rich surface oxides with aluminum-rich internal oxides forming below the sample's surface.<sup>[6-9]</sup> The corrosion reactions discovered in these studies showed that the industrial application of these alloys at temperatures greater than 1173 K (900 °C) in impure helium will be limited by oxidation.

Due to the great potential of NGNPs, there have been many scientific studies devoted to understanding how the high-temperature and impure helium environment of VHTR affect the long-term mechanical properties of the above-mentioned candidate alloys. In recent years, significant findings have shed light on creep rupture, fatigue strength, crack growth rate, and creep fatigue, exploring the effects of impure helium corrosion on material properties. Because Alloy 617 is the most promising alloy candidate, the majority of impure helium mechanical testing was performed using this material. Early tensile testing showed a loss of ductility in Alloy 617 samples aged in impure helium environments, while creep testing determined that the creep rupture time for Alloy 617 was much shorter in an impure helium environment than in standard air for the same temperature.<sup>[10-12]</sup>

After a basic understanding of how a VHTR's environment affects structural alloys was gained, more intricate low-cycle fatigue and creep fatigue experiments were performed on Alloy 617 and Haynes 230. These experiments revealed that oxidation caused by the impure helium environment accelerated the initiation of intergranular cracking and crack growth, which resulted in a significant reduction in the material's fatigue life.<sup>[13,14]</sup> It was also found that creep stress does not significantly influence the creep void fraction at a given tested creep strain, and void formation occurred only after significant creep in the tertiary regime had occurred.<sup>[15]</sup> A fatigue crack propagation (FCP) and sustained loading crack growth (SLCG) study concluded that the linear elastic fracture mechanism parameter, stress intensity factor ( $K$ ), is sufficient to describe the FCP and SLCG behavior at testing temperatures ranging from 873 K (600 °C) to 1073 K (800 °C).<sup>[16]</sup> This study also determined that the stress-assisted grain boundary oxygen embrittlement mechanism is mainly responsible for the accelerated time-dependent FCP rates of both Inconel 617 and Haynes 230. Additionally, in creep fatigue crack growth experiments performed by Benz and Wright on Alloy 617, the crack growth was found to be primarily intergranular, and creep crack growth rates were higher in the impure helium environment than in air.<sup>[17]</sup>

The research reported below evaluates the role of impurities in helium coolant on the stress-assisted grain boundary oxidation and creep crack growth in candidate Alloys 617 and 800H at elevated temperatures, similar to the environments found in VHTR. Creep crack growth rates of these candidate alloys are measured in air and in impure helium, and the effects of oxygen impurities in helium on the stress-assisted grain boundary oxidation and creep crack growth are evaluated within the range stipulated by the NGNP program.<sup>[18]</sup> Furthermore, this research evaluates the effects of a particular method of grain boundary engineering on the mitigation of stress-assisted grain boundary oxidation and creep crack growth.

## II. MATERIALS AND METHODS

### A. Materials and Specimens

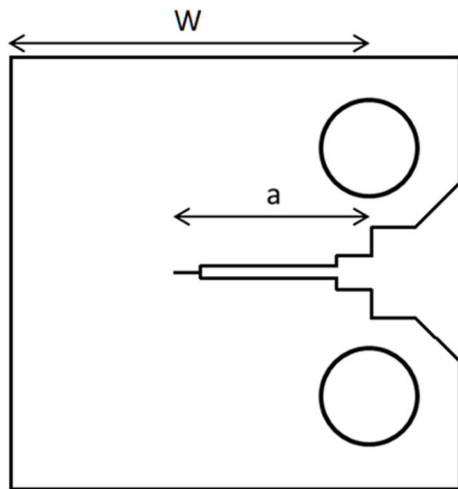
Two candidate alloys were studied in detail: Alloy 617 and Alloy 800H. Alloy 617 is the leading candidate alloy for intermediate heat exchangers. It has been reported that Alloy 617 can be used at temperatures as high as 1255 K (982 °C).<sup>[19]</sup> Alloy 800H is currently approved under ASME code for nuclear service for up to 1033 K (760 °C) and could be immediately used in a lower-temperature reactor.

Table I presents the chemical compositions of the as-received alloys. All 617 and 800H samples used in these studies were provided by Idaho National Laboratory, Idaho Falls, Idaho, USA. The materials were cut from much larger ingots. Before the creep crack growth testing, both Alloy 617 and Alloy 800H were solution-treated (ST) at 1473 K (1200 °C) for one hour and then quenched in water, as suggested by Special Metals.<sup>[20]</sup> Because the Alloy 617 and Alloy 800H materials will be used ultimately for extended periods of time and at high temperatures during heat exchanger service, the materials were further heated to 1123 K (850 °C) for 2000 hour in air to age the materials. During the aging process, small coupons of the candidate alloys were removed at specific time intervals. Hardness and tensile testing of the aged coupons were performed to evaluate the mechanical properties of the alloys as a function of aging time (testing details to follow). Rolling direction was tracked through all stages of sample preparation.

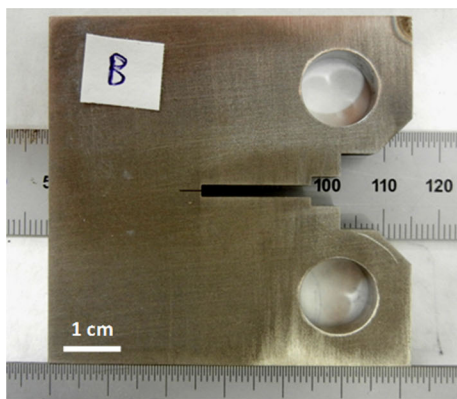
Compact tension (CT) specimens for the creep crack growth (CCG) experiments were fabricated from the alloy materials per CT specimen geometry defined by ASTM standard E1457-13.<sup>[21]</sup> After an investigation into the necessary stress levels needed to induce creep crack growth within the candidate alloys, along with a comprehensive evaluation of the anticipated stress levels in the load-bearing components of the CCG testing apparatus, design values of  $W = 50$  mm,  $a = 27.5$  mm (shown in Figure 1(a)), and  $B = 6.25$  mm (thickness) were chosen for the CT specimens. Electric discharge machining (Japax EDM) was used to fabricate the CT specimens, with the orientation of the crack being aligned with the rolling direction of the samples (Figure 1(b)). Fine-wire EDM performed by Integrity

**Table I. Actual Chemical Compositions of the Tested Alloys**

Element Alloy	Ni	Cr	Fe	Co	Mo	Ti	Al	C	Si	Mn	Cu	P	B	S
Alloy 617	54.1	22.2	1.6	11.6	8.6	0.4	1.1	0.05	0.1	0.1	0.04	—	<0.001	<0.002
Alloy 800H	30.65	19.7	46.24	0.1	—	0.54	0.56	0.061	0.42	1.27	0.2	0.024	—	0.001



(a)



(b)

Fig. 1—(a) Schematic of compact tension specimen geometry defined by ASTM standard E1457-13 ( $W = 50$  mm,  $a = 27.5$  mm). (b) Photograph of an Inconel 617 compact tension specimen used in this study ( $W = 50$  mm,  $a = 27.5$  mm).

Wire EDM Inc. (Sussex, Wisconsin) was used to machine the final 3.75-mm length of the crack at a width of  $\sim 100$   $\mu\text{m}$ .

### B. Grain Boundary Engineering

Grain boundary engineering (GBE) and microstructure characterization of GBE samples were performed by Integran Technologies (Mississauga, Ontario, Canada). The GBE optimization was performed on as-received (*i.e.*, not solution-treated and not aged) Alloy 617 samples. The GBE processing, which involves repeated room temperature cold rolling deformation and annealing cycles, was conducted per US Patents 5,702,543 and 6,129,795. This processing creates

annealing twins and low  $\Sigma$  special grain boundaries through the formation of annealing twins during early-stage recrystallization. The pre-strain applied was less than 30 pct; annealing was carried out in air furnace at 1273 K to 1373 K (1000  $^{\circ}\text{C}$  to 1100  $^{\circ}\text{C}$ ) for short duration ( $<10$  min at temperature); and cooling was conducted in air.<sup>[22]</sup>

### C. Creep Crack Growth (CCG) Testing and Apparatus

An apparatus for conducting CCG experiments on candidate alloys at elevated temperatures was developed to perform testing in prototypical environments according to the requirements established in ASTM standard E 1457-13.<sup>[21]</sup> The apparatus was designed for testing three CT specimens in series within an environmental chamber and under dead-weight loading.<sup>[23]</sup> The direct current potential drop (DCPD) technique was employed to monitor crack growth continuously during testing. Figure 2 presents a schematic of the overall CCG test apparatus and data acquisition system.

The composition of the impure helium, a custom premixed and certified by the vendor (Airgas, Inc., Madison, WI), used for these CCG studies is presented in Table II. The compressed air “Air, Zero Grade” was composed of nitrogen (78 to 80 pct) and oxygen (20 to 22 pct), with  $\leq 3$  ppm  $\text{H}_2\text{O}$  and  $\leq 1$  ppm total hydrocarbon content (Airgas, Inc., Madison, WI). Details of CCG test apparatus, environmental control, and mass spectroscopy analysis have been described previously.<sup>[23]</sup>

### D. Metallographic Analysis

After CCG testing was complete, EDM cuts were made through the CT specimens in the direction of the crack at a depth of  $B/2$  to reveal the interior of the samples. Each slice was then ground using 240, 600, 800, and 1200 grit SiC paper, followed by a final polishing using 0.05  $\mu\text{m}$  colloidal silica. The polished samples were then ultrasonically cleaned in acetone for 3 to 5 minutes. Each sample was examined by scanning electron microscopy (SEM) to image the interior crack at high resolution. Electron backscatter diffraction (EBSD) was used to examine the crystallographic orientations of the samples and to evaluate the misorientation of grains and the strain near the cracks.

The SEM images of the interior of the samples were used to assess crack morphology and to quantify crack length. All final crack lengths were taken to be the projected length of the longest crack that propagated into the sample along the direction of the precrack. A custom MATLAB code was used to trace the boundaries of all the cracks in order to quantify the actual lengths of the individual cracks as well as the bounding

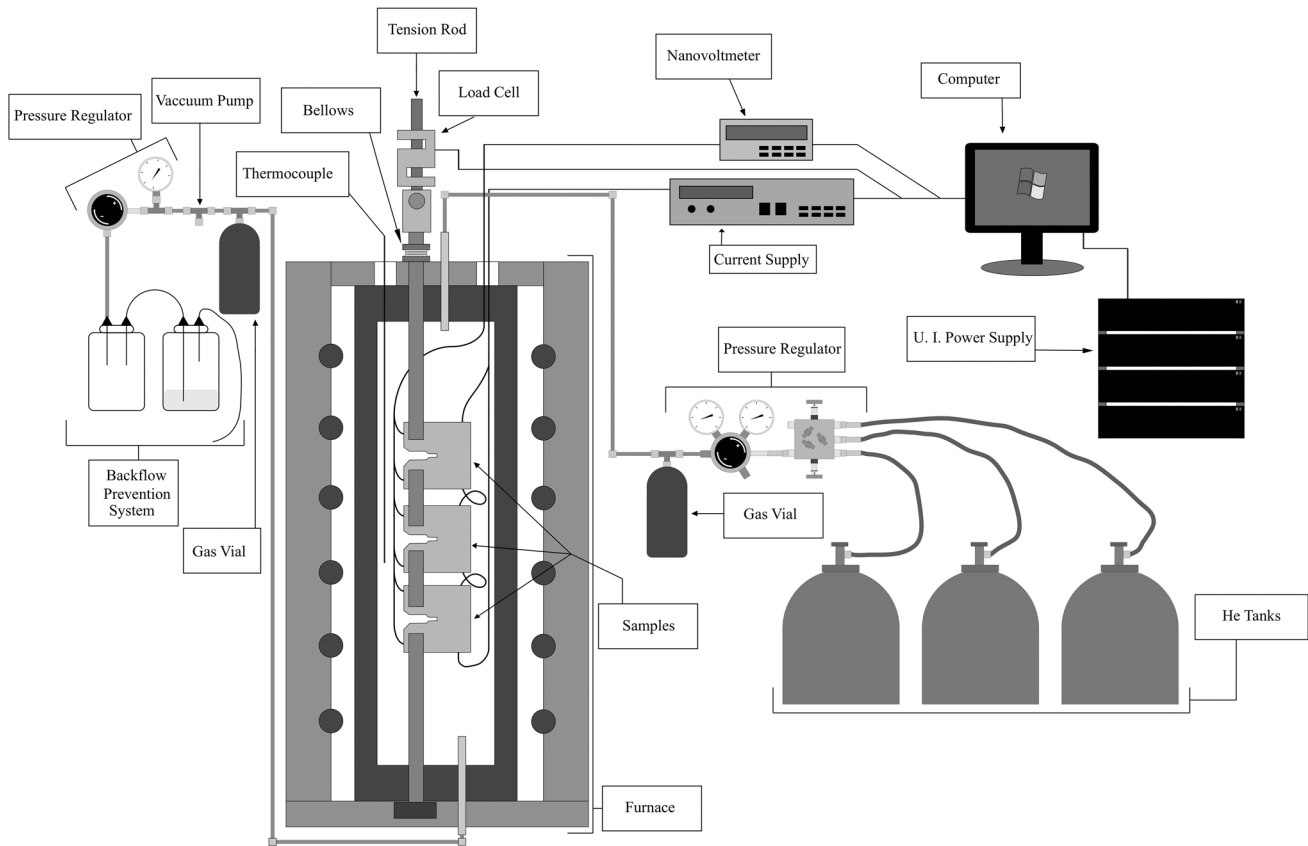


Fig. 2—Schematic depiction of the key components of the creep crack growth (CCG) testing apparatus. Reprinted with permission from Ref. [23].

**Table II. Composition of Impure Helium Used for These Studies**

Gas	Composition (ppm)
Carbon monoxide	12
Carbon dioxide	1.5
Oxygen	0.5
Nitrogen	0.5
Argon	0.5
Water vapor	0.2

area that encompassed all cracks. The tracing of each crack was done manually by selecting one face of an individual crack and following that face within the resolution limits of the SEM image (on the order of  $\mu\text{m}/\text{pixel}$ ). The bounding area was defined as the polygon with the least number of sides that encompassed all cracks and intersected the precrack at a predetermined reference distance behind the original notch tip ( $300\ \mu\text{m}$  for all samples studied here). The custom code yielded the following information: projected length of the longest crack, number of individual cracks, actual length of each crack, total length of all cracks, and bounding area that encompassed all cracks. Because all samples were sectioned in half, results were recorded for both sides of the central plane, and the data reported in the following represent the average of the results obtained from measuring each side of the

sample. A sample crack measurement is shown in Figure 3.

### III. RESULTS AND DISCUSSIONS

#### A. Crack Measurement Results

SEM images of the interiors of the CT specimens revealed that the longest interior crack was longer than the longest exterior crack in all cases. Therefore, the length of the longest crack within the interior of each specimen was used to quantify crack growth during CCG testing. Additionally, many crack branches were readily observed within the samples' interiors. The total number of cracks,  $N_{\text{cracks}}$ , and the bounding area that encompassed all cracks were measured to quantify the extent of damage produced by CCG testing in different environmental conditions. A plot of the number of cracks vs the bounding area normalized by the longest projected crack length for all three samples tested under each condition is shown in Figure 4. A general overall trend is observed whereby the samples with a large number of cracks exhibited cracks that were spread out over a relatively large area compared to the length of the longest crack, and, in the samples with fewer cracks, the cracks were contained to a relatively small area compared to the length of the longest crack. The plot shown in Figure 4 also reveals that, on average, the Alloy 800H samples tested at 973 K ( $700\ ^\circ\text{C}$ ) exhibited fewer cracks, with those cracks being spread out over a relatively smaller area, compared to the Alloy 617 samples.

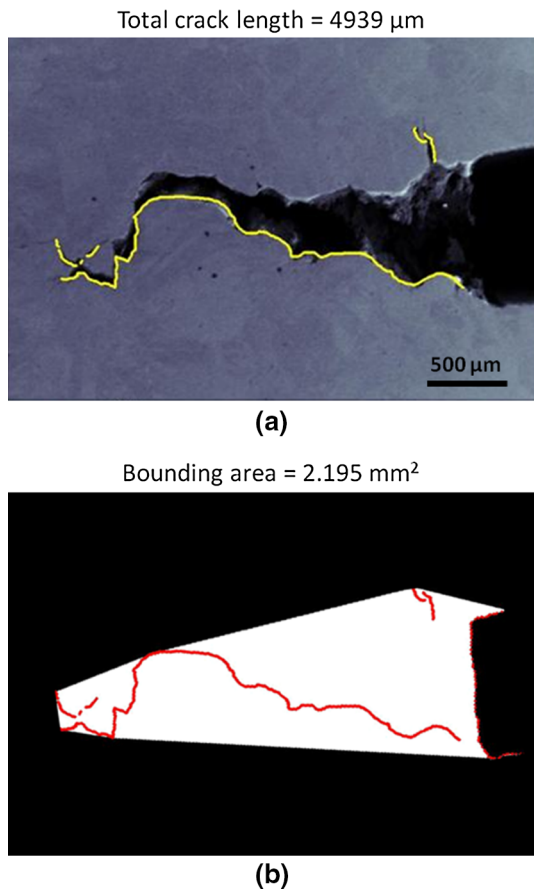


Fig. 3—Example of crack tracing results showing tracing of the crack to determine total length of the crack surfaces (a) and the bounding area that includes all cracks (b).

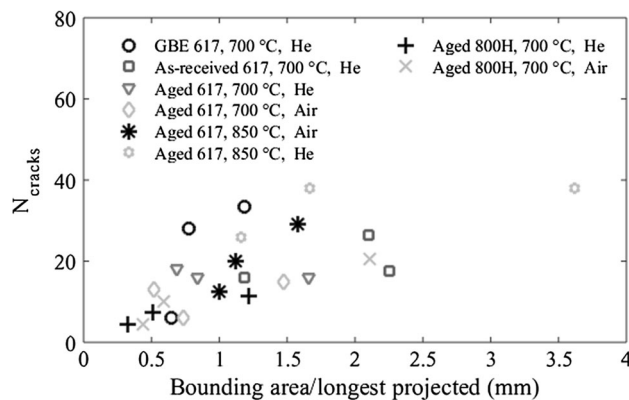


Fig. 4—Damage produced by CCG testing in different environmental conditions shown as a plot of the number of cracks produced in the interior surface of the sample vs the bounding area normalized by the projected length of the longest crack.

## B. Microscopy Results

SEM images of the crack morphologies of Alloy 617 tested at 973 K (700 °C) in air showed one major crack. There were many small crack branches in Alloy 617 samples tested at 973 K (700 °C) in helium. In both air and helium, some small crack initiations and/or

cavitations were observed in front of the crack tip. Crack propagation along the grain boundaries was readily observed. It appears that the cracks initiated primarily from the triple point grain boundary junctions and in the vicinity of the carbide phases. EDS analysis of oxidation at the crack for Alloy 617 tested in both conditions was similar, with the oxide consisting mainly of chromium oxide, although there was an aluminum-rich phase present in Alloy 617 tested in He.

Crack morphologies from Alloy 617 tested at 1123 K (850 °C) in air and helium were similar, namely, there was one major crack accompanied by many small cracks. In both cases, the cracks were intergranular, and cracks appeared to have initiated from the triple point grain boundary junctions and carbide regions. Additional data on the intergranular nature of these cracks have been described previously.<sup>[24]</sup> Compared to Alloy 617 tested at 973 K (700 °C), a larger amount of oxidation in Alloy 617 tested at 1123 K (850 °C) in air and helium was observed. In addition, aluminum oxide phases were formed in the inner oxidation layer and along some of the grain boundaries at 1123 K (850 °C) (Figures 5 and 6).

SEM images of the crack morphologies in the Alloy 800H samples tested at 973 K (700 °C) in air and in helium revealed one major crack in each sample. The cracks propagated along the grain boundaries and around the carbide phases. EDS mapping of the cross sections of the oxide layers of Alloy 800H tested at 973 K (700 °C) in air and in helium showed that the amount of oxidation was significantly higher in Alloy 800H tested in air. The outer layer is an iron oxide, and the inner layer is a chromium oxide. In Alloy 800H tested in helium, however, the oxidation layer is mainly chromium oxide.

The GBE processing protocols developed by Integran Technologies were successful in facilitating multiple twinning leading to an elevated frequency of special grain boundary content and enhanced special grain boundary connectivity at local triple junctions. Compared to the material in the as-received condition, the microstructural characteristics of the GBE-optimized samples had a grain size of  $\sim 30 \mu\text{m}$ , an enhanced 'special' (*i.e.*,  $\Sigma \leq 29$ ) grain boundary frequency in the range of  $\sim 70$  pct with a significant increase in the presence of twin variant interfaces (*i.e.*,  $\Sigma 9$  and  $\Sigma 27$ ), and an improved grain boundary network connectivity, which is evidenced by the increase in the frequency of triple junctions with three special grain boundaries.<sup>[22]</sup> After CCG testing of the GBE processed and as-received Alloy 617 samples at 973 K (700 °C) in helium, SEM analysis showed much more severe cracking in GBE-processed samples as compared to the aged samples described above. The cracks appear to be intergranular, and many crack branches are observed in the GBE samples. In addition, an aluminum-rich phase is observed in both the GBE and as-received samples.

After SEM imaging, samples of each type were pulled apart at room temperature after the CCG testing to examine the fracture surfaces. Oxide decoration allowed easy identification of the CCG fracture surface. In all cases, the major crack was continuous from one side of

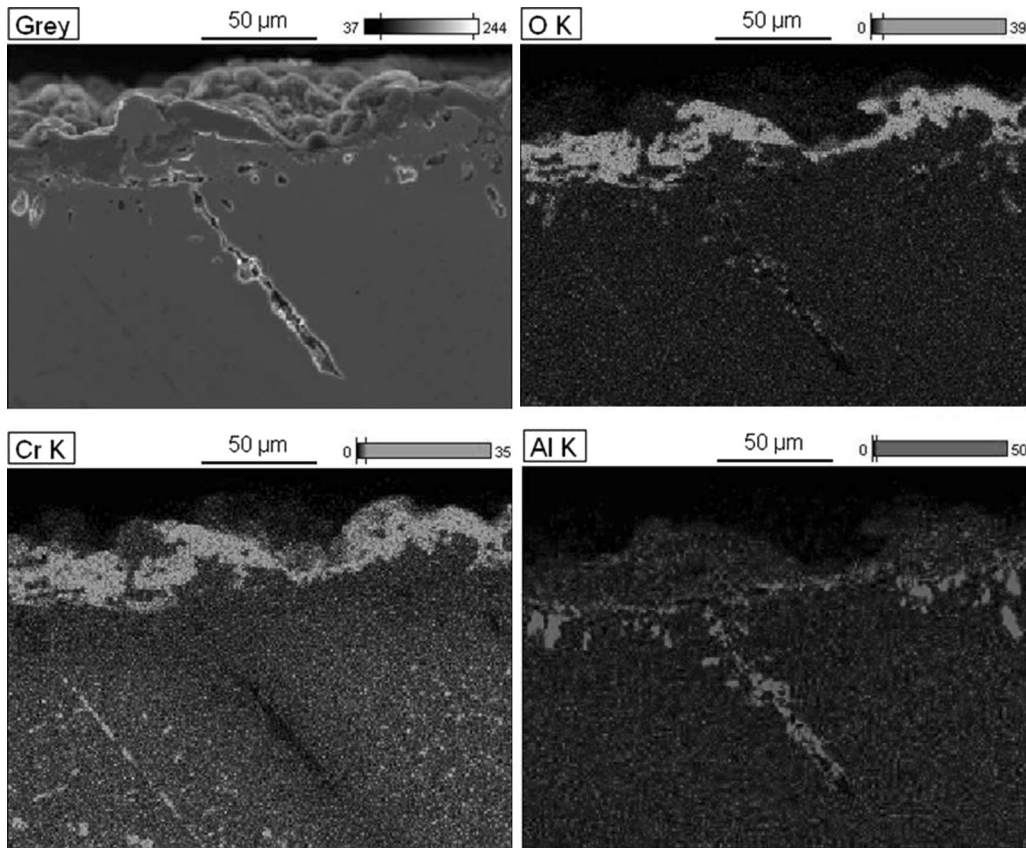


Fig. 5—EDS mapping of Alloy 617 tested at 1123 K (850 °C) in air. Aluminum-rich oxide phases are observed on the surface and along some of the grain boundaries.

the sample to the other, and the longest crack occurred in the center of the sample. Microscopy on the fracture surfaces determined that all cracks were intergranular.

### C. CCG Results

For all CCG tests, the direction of crack propagation was parallel to the rolling direction, and the cracks were prevented from propagating entirely through the samples in order to quantify the final crack length for the calibration of the DCPD measurements. All final crack lengths were measured *via* SEM by cutting each CT specimen in half and measuring the projected length of the longest crack within the interior of the specimen. The forthcoming CCG curves for all but two of the tests comprise the data points from all three CT specimens. Due to minimal crack growth within one sample from the Alloy 617 test at 973 K (700 °C) in He and one sample from the Alloy 617 test at 1123 K (850 °C) in He, those curves comprise the data points from the two remaining specimens in the test set.

The CCG results from the Alloy 617 samples tested at 973 K (700 °C) are presented in Figure 7. Results for  $da/dt$  vs  $K_I$  for the 617 samples tested at 973 K (700 °C) reveal that aged Alloy 617 samples tested in air exhibit the highest resistance to crack growth, followed by the aged 617 samples tested in helium, followed by the as-received 617 samples tested in helium, followed by

GBE samples tested in helium. Grain boundary engineering of the 617 alloy produced inferior CCG results compared to both aged and as-received 617 samples, although other mechanical properties such as strength and hardness were clearly superior (see Supplemental Data on Mechanical Properties).

The CCG results from the Alloy 617 samples tested at 1123 K (850 °C) are presented in Figure 8. The aged 617 samples tested at 1123 K (850 °C) show a dramatic reduction in resistance to crack growth compared to the samples tested at 973 K (700 °C); *e.g.*,  $K_I \approx 4 \text{ MPa}\sqrt{\text{m}}$  gives rise to crack growth at 1123 K (850 °C), whereas  $K_I > 15 \text{ MPa}\sqrt{\text{m}}$  is required to induce cracking at 973 K (700 °C). At 1123 K (850 °C), the crack growth resistance appears to be slightly better in the He environment, although the early spike in  $da/dt$  around  $K_I \approx 4 \text{ MPa}\sqrt{\text{m}}$  (only measured in one of the samples tested in He) indicates that the crack growth rate accelerated initially but then slowed as that test progressed. Comparing the results from 973 K and 1123 K (700 °C and 850 °C), the significant reduction in the crack growth resistance of the 617 samples tested at the higher temperature is correlated with the known dramatic reductions in creep resistance and strength, both of which likely lead to the pronounced reduction in crack growth resistance.

The CCG results from the Alloy 800H samples tested at 973 K (700 °C) are presented in Figure 9. The 800H

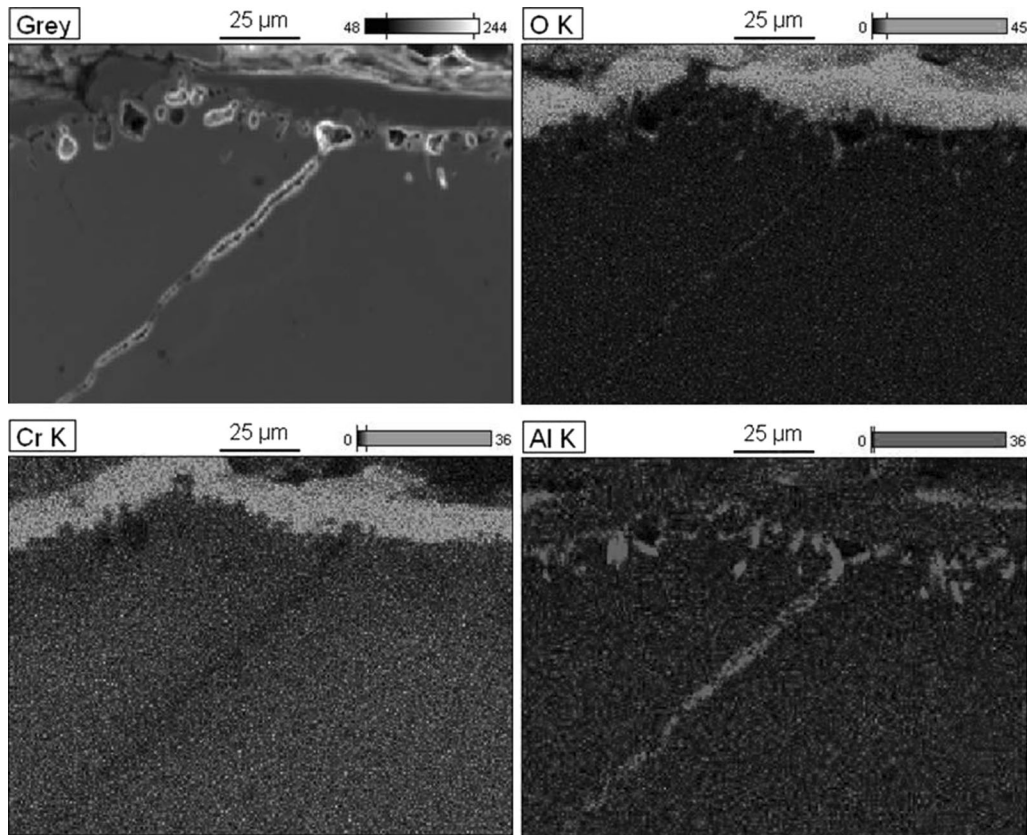


Fig. 6—EDS mapping of Alloy 617 tested at 1123 K (850 °C) in helium. Aluminum-rich phases are observed on the surface and along some of the grain boundaries.

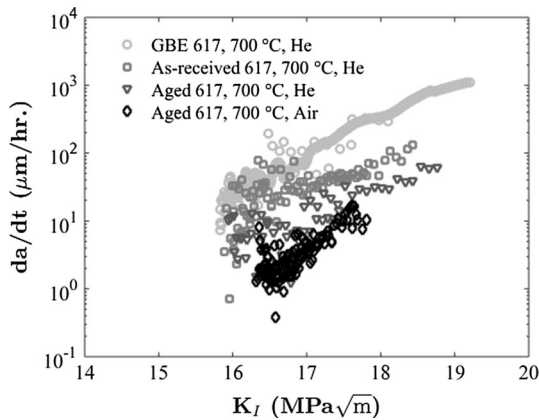


Fig. 7—CCG results for Alloy 617 tested at 973 K (700 °C).

samples tested in air at 973 K (700 °C) exhibit a resistance to crack growth that is substantially worse than all results obtained from the 617 samples tested at 973 K (700 °C), with performance that is only marginally better than that of the 617 samples tested at 1123 K (850 °C); *e.g.*,  $K_I \approx 5 \text{ MPa}\sqrt{\text{m}}$  produces crack growth in Alloy 800H tested at 973 K (700 °C), whereas  $K_I \approx 4 \text{ MPa}\sqrt{\text{m}}$  produces cracking in Alloy 617 at 1123 K (850 °C). The crack growth resistance for 800H appears to be slightly better in the air environment as compared to He. The inferior CCG performance of

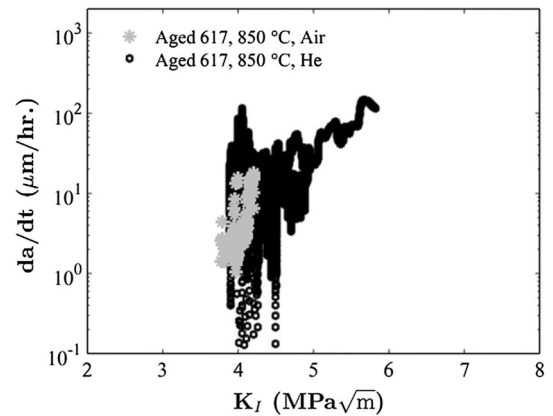


Fig. 8—CCG results for Alloy 617 tested at 1123 K (850 °C).

Alloy 800H is correlated with the inferior mechanical properties measured (see Supplemental Data on Mechanical Properties). Figure 10 presents all the results from the CCG tests conducted with Alloys 617 and 800H in air and in impure He.

#### IV. DISCUSSION

The results reported above show the creep crack growth characterization of Alloys 617 and 800H at elevated temperatures in air and in impure helium

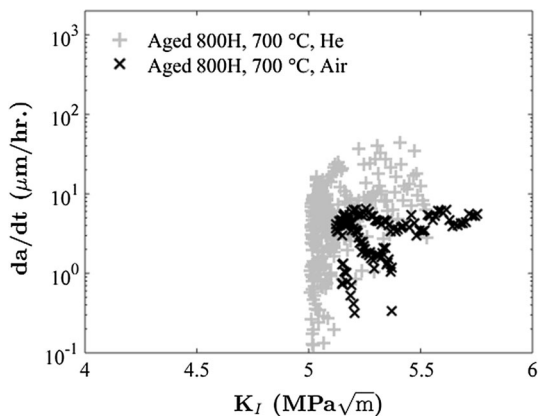


Fig. 9—CCG results for Alloy 800H tested at 973 K (700 °C).

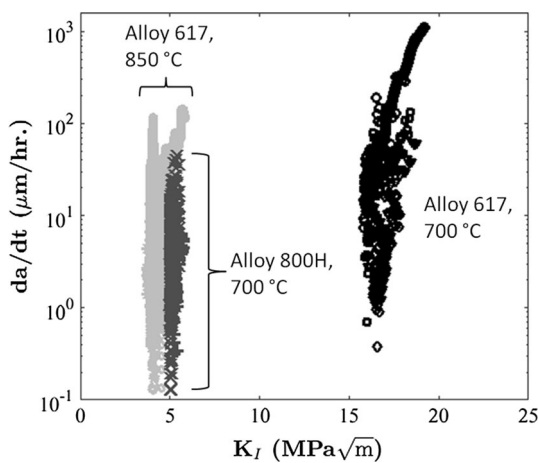


Fig. 10—CCG results for all alloys and conditions tested.

environments. Alloy 617 appears to have similar oxidation behavior in both environments, with a very thin oxidation layer forming on the surface of the alloy. This may explain the similarity in the creep crack growth rates of Alloy 617 tested in air and in impure helium. When Alloy 617 is tested at 1123 K (850 °C), the degree of oxidation on the surface is much more severe, and again the oxidation in the air and helium environments is similar. In both environments, there is significant formation of aluminum oxide phases along the inner oxidation layer and along a number of grain boundaries. Alloy 800H shows slight differences in oxidation in air compared to helium. When Alloy 800H was tested in air, the outer layer was iron oxide, and the inner layer was chromium oxide. However, when tested in helium, the oxidation layer was mainly composed of chromium oxide.

The poorer CCG performance for the grain boundary engineered samples was unexpected, given that this material had shown superior hardness and strength in supplemental testing. However, in the as-received Alloy 617 samples, the grains are significantly smaller than those of the aged samples, and the grains of the GBE Alloy 617 samples are smaller than those of the as-received samples. These differences present a

confounding factor for the direct comparison of CCG test results for the different 973 K (700 °C) tests conducted on Alloy 617 samples. However, it is notable that the GBE samples had lower creep crack growth resistance compared to all other Alloy 617 samples tested at 973 K (700 °C), despite the fact that GBE was shown to have a positive impact on other material properties. From the comparison of the microstructure of the as-received (solution annealed) and aged Alloy 617, there are more grain boundary chromium carbides in the aged samples. During the process of creep crack propagation, the crack generally propagated around these carbides. This suggests that the grain boundary carbides may be beneficial for the creep crack growth performance. In the GBE Alloy 617, the grain boundary carbides were broken during the multiple cold rolling processes. This may have contributed to the lower creep crack growth resistance of the GBE samples.

In all Alloy 617 samples tested in air or helium, the creep cracks propagated along the grain boundaries. Grain boundaries are generally weaker in mechanical strength as compared to the nearby grains. The larger the grain size, the greater the distance needed for the crack to propagate along the grain boundaries, and the cracks appear more serrated as compared to the cracks in fine-grained samples.

A thin chromium oxide layer is observed in both the as-received and GBE samples, as is a small amount of an aluminum-rich phase. The long axis of the grains is observed to be parallel to the stress direction during testing. Grain size appears to have a significant effect on the creep crack growth rates in these candidate alloys. Both the GBE and the as-received Alloy 617 samples have much higher crack growth rates compared to the aged Alloy 617 samples tested in the same helium environment and at the same temperature, with the GBE samples having the lowest resistance to crack growth among the samples tested at 973 K (700 °C). It is therefore concluded that the samples with smaller grains have decreased resistance to creep and therefore exhibit a reduction in crack growth resistance. Future studies would be required to understand the dependence of crack growth resistance within GBE samples on the direction of crack propagation.

## V. CONCLUSIONS

Resistance to creep crack growth has been explored for candidate alloys 617 and 800H. CCG testing of both alloys revealed that, overall, Alloy 617 has superior resistance to creep crack growth compared to that of Alloy 800H. CCG testing at 973 K (700 °C) demonstrated that Alloy 617 has a higher resistance to creep crack growth in air compared to impure helium, while the CCG results for Alloy 800H suggest that air and helium environments produce similar behavior. CCG testing of grain boundary-engineered (GBE) Alloy 617 samples revealed that this technique produces inferior resistance to creep crack growth compared to the other Alloy 617 samples tested under similar conditions.



Grain size was found to correlate positively with resistance to creep crack growth, with the GBE samples having the smallest grain size of the Alloy 617 samples tested. Future work will involve explorations into the nature of the relationship between grain size of Alloy 617 and resistance to slow crack growth at elevated temperatures, and GBE processing conditions will be further investigated to determine the degree to which the special grain boundaries provide resistance to crack initiation and propagation in Alloy 617.

## ACKNOWLEDGMENTS

The authors wish to thank Jacob Jelinek and Paul Roman for mass spectroscopy assistance, Dr. Shiluo Yan for assistance with electrical measurements, and Brett Napiwocki for performing the manual crack tracing for measuring crack lengths. This research was performed using the funding provided by the U.S. Department of Energy Office of Nuclear Energy's Nuclear Energy University Programs under Battelle Energy Alliance, LLC Standard Research Contract No. 00088925, entitled "Assessment of Embrittlement of Very High Temperature Reactor Structural Alloys in Impure Helium Environments," to the University of Wisconsin, under Prime Contract No. DE-AC07-05ID14517.

## ELECTRONIC SUPPLEMENTARY MATERIAL

The online version of this article (doi:[10.1007/s40553-016-0102-0](https://doi.org/10.1007/s40553-016-0102-0)) contains supplementary material, which is available to authorized users.

## REFERENCES

1. S. Badwal, S. Giddey, and C. Munnings: *WENE*, 2013, vol. 2 (5), pp. 473–87.
2. D.L. Youchison, M.T. North, J.E. Lindemuth, J.M. McDonald, and T.J. Lutz: *Fusion Eng. Des.*, 2000, vol. 49, pp. 407–15.
3. D. Morgan and K. Sridharan: Report Number ORNL/TM-2008/129, Oak Ridge National Laboratory, August 2008.
4. R. Wright, J. Simpson, A. Wertsching, and W.D. Swank: *Proceeding of the Fourth International Topical Meeting on High Temperature Reactor Technology*, 2008, pp. 75–79.
5. T. Allen, H. Bulet, R.K. Nanstad, M. Samaras, and S. Ukai: *MRS Bull.*, 2009, vol. 34, pp. 20–27.
6. C. Jang, D. Lee, and D. Kim: *Int. J. Press. Vessels Pip.*, 2008, vol. 85 (6), pp. 368–77.
7. D. Kumar, R.R. Adharapurapu, T.M. Pollock, and G.S. Was: *Metall. Mater. Trans. A*, 2011, vol. 42 (5), pp. 1245–65.
8. C. Cabet and B. Duprey: *Nucl. Eng. Des.*, 2012, vol. 251, pp. 139–45.
9. G.G. Lee, S. Jung, D. Kim, Y.W. Jeong, and D.J. Kim: *Nucl. Eng. Des.*, 2014, vol. 271, pp. 301–08.
10. P.S. Shankar and K. Natesan: *J. Nucl. Mater.*, 2007, vol. 366 (1), pp. 28–36.
11. D. Kim, I. Sah, and C. Jang: *J. Nucl. Mater.*, 2010, vol. 405 (1), pp. 9–16.
12. W.G. Kim, G.G. Lee, J.Y. Park, S.D. Hong, and Y.W. Kim: *Procedia Eng.*, 2013, vol. 55, pp. 819–22.
13. C. Cabet, L. Carroll, and R. Wright: *J. Press Vessel Technol.*, 2013, vol. 135 (6), p. 061401.
14. X. Chen, Z. Yang, M.A. Sokolov, D.L. Erdman, K. Mo, and J.F. Stubbins: *J. Nucl. Mater.*, 2014, vol. 444 (1), pp. 393–403.
15. L.J. Carroll, C. Cabet, R. Madland, and R. Wright: *Journal of ASTM International*, 2011, vol. 8, No. 6, pp. JA1103797, Report Number: INL/JOU-11-20890, Idaho National Laboratory.
16. L. Ma, S.K. Roy, M.H. Hasan, J. Pal, and S. Chatterjee: *Metall. Mater. Trans. A*, 2012, vol. 43A (2), pp. 491–504.
17. J.K. Benz and R.N. Wright: Report Number: INL/CON-13-30214, Idaho National Laboratory, October 2013.
18. Center for Advanced Energy Studies, Idaho National Laboratory, Nuclear Energy University Programs Research Needs, p. 35. December 2008.
19. J. M. Corum and J. J. Blass: American Society of Mechanical Engineers (ASME) pressure vessels and piping conference; San Diego, CA, June 1991, CONF-91062-30. Accessible from the International Nuclear Information System Repository, International Atomic Energy Agency, Vienna, Austria, [http://www.iaea.org/inis/collection/NCLCollectionStore/\\_Public/22/085/22085754.pdf](http://www.iaea.org/inis/collection/NCLCollectionStore/_Public/22/085/22085754.pdf). Accessed 5 June 16.
20. Special. Metals: *Corporation*, New York, personal communication, New Hartford, 2009.
21. ASTM Standard E1457-13, Standard Test Method for Measurement of Creep Crack Growth Times and Rates in Metals, ASTM International, West Conshohocken, PA, 2013. [www.astm.org](http://www.astm.org).
22. Integran Technologies, Final Report: Fabrication and Characterization of Grain Boundary Engineered (GBE™) IN617 Test Samples. Project Number: 2011-UWI-602-0585, 2009, pp. 1–14.
23. D. Grierson, G. Cao, P. Brooks, P. Pezzi, A. Glauddell, D. Kuettel, G. Fisher, T. Allen, K. Sridharan, and W.C. Crone: *Exp. Mech.*, 2015, vol. 55 (2), pp. 417–26.
24. D. Grierson, G. Cao, A. Glauddell, D. Kuettel, G. Fisher, P. Pezzi, P. Brooks, T. Allen, K. Sridharan, and W.C. Crone: *Fract. Fatigue Fail. Damage Evol.*, 2015, vol. 5, pp. 203–09.